CRYSTAL GROWTH & DESIGN

Article

pubs.acs.org/crystal

3,6-Connected Metal–Organic Frameworks Based on Triscarboxylate as a 3-Connected Organic Node and a Linear Trinuclear $Co_3(COO)_6$ Secondary Building Unit as a 6-Connected Node

Dongwook Kim,[†] Xiaokai Song,[†,‡] Jung Hee Yoon,[†] and Myoung Soo Lah*[,†]

[†]Interdisciplinary School of Green Energy, Ulsan National Institute of Science & Technology, Ulsan 689-805, Korea

[‡]Department of Chemistry and Applied Chemistry, Hanyang University, Ansan, Kyunggi-do 426-791, Korea

Supporting Information

ABSTRACT: The solvothermal reactions of cobalt(II) chloride hexahydrate and 1,3,5-benzenetribenzoic acid (H_3BTB) in anhydrous *N*,*N*′-dimethylacetamide (DMA) at two different reaction temperatures and reactant concentrations led to two 3,6-connected metal–organic frameworks (MOFs) with different net topologies based on the ligand as a C_3 symmetric 3-connected organic node and the linear trinuclear cobalt carboxylate cluster, $Co_3(COO)_6$, as a 6-connected secondary building unit (SBU). MOF $[Co_3(BTB)_2(DMA)_4]$, **1**, with a linear trinuclear cobalt carboxylate cluster, $Co_3(COO)_6$, and with an inversion point symmetry with "compressed trigonal antiprismatic" 6-connectivity, is a two-dimensional (2-D) layered structure of a 3,6-connected **kgd** net topology. However, the same linear trinuclear cobalt carboxylate cluster, $Co_3(COO)_6$, with a 2-fold point symmetry with "compressed trigonal prismatic" 6-connectivity leads to the three-dimensional (3-D) network of **2**, with an unprecedented 3,6-connected net topology with the point symbol $(4^3)_2(4^3{\cdot}12^{12})$. The 2-D layered framework, **1**, shows a significant sorption hysteresis for adsorbates with relatively strong interactions with the framework, such as N_2 and CO_2.

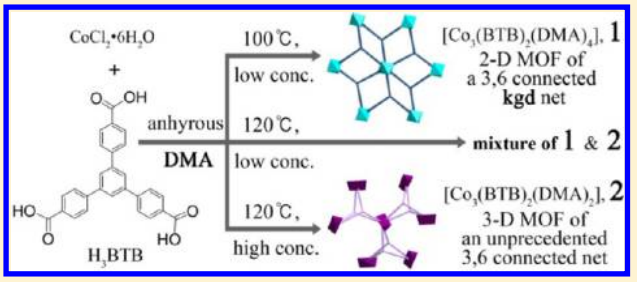

INTRODUCTION

It is a very difficult task to design and predict a new metal–organic framework (MOF) structure with a specific net topology from the metal ion and organic linker used as the reactants. The same reactants can result in completely different framework structures, depending on the reaction conditions used, such as solvent, temperature, concentration and ratio of reactants, reaction time, and pH.

Rigid building blocks with a specific connectivity and local point symmetry can increase the predictability of the final network structure, because the constrained interconnectivity of the building blocks leads to networks with a limited number of net topologies.[1] MOF-5 and its isoreticular structures are obtained as networks with a 6-connected **pcu** net topology, where 6-connected octahedral $Zn_4O(COO)_6$ secondary building units (SBUs) are interconnected via various rigid linear ditopic organic linkers.[2] HKUST-1 and its isoreticular structures[3] are also obtained as networks with a 3,4-connected **tbo** net topology,[4] where square planar 4-connected $Cu_2(COO)_4$ paddle wheel SBUs are interconnected via various rigid 3-connected organic nodes.

1,3,5-Benzenetribenzoic acid (H_3BTB) is one of the most widely used ligands as a rigid nonplanar C_3 symmetric 3-connected organic node, with various metal ions having a diverse connectivity and local point symmetry in the design of MOF structures.[5−7] For example, in contrast to the rigid C_3 symmetric 3-connected trisbenzoic acid with three carboxylic acid residues in the ligand plane in HKUST-1 with a 3,4-connected **tbo** net topology, the same C_3 symmetric but nonplanar 3-connected H_3BTB with three carboxylic acid residues twisted in the ligand plane reacts with Cu(II) ions to generate MOF-14,[6a] having the same 3,4-connectivity but with a **pto** net topology, based on a square planar $Cu_2(COO)_4$ paddle wheel as a 4-connected SBU.[4] When 3-connected 1,3,5-benzenetribenzoate (BTB) is combined with an octahedral 6-connected $Zn_4O(COO)_6$ SBU, then MOF-177, having a 3,6-connected **qom** net topology, is obtained.[5a] The net topologies of these MOF structures are predetermined by the connectivity and the local point symmetries of the rigid building blocks, or at least, the number of the allowed net topologies is limited.

On the other hand, it is more difficult to predict or design an MOF composed of cobalt carboxylate clusters as an SBU because Co(II) ions do not have a strong preference for a specific cobalt carboxylate cluster with a defined connectivity and a point symmetry. Depending on the reaction conditions, MOFs (or coordination polymers) with a diverse net topology are obtained, where the MOFs contain various cobalt carboxylate clusters as SBUs with a diverse connectivity and local point symmetry.[8−12] However, a linear trinuclear cobalt cluster with six bridging carboxylate groups, $Co_3(COO)_6$, is still

Received: May 18, 2012
Revised: June 13, 2012
Published: June 18, 2012

dx.doi.org/10.1021/cg300686n | *Cryst. Growth Des.* 2012, 12, 4186–4193

one of the most frequently occurring structural units as a potential 6-connected node, and the number of possible local point symmetries of the linear trinuclear cobalt cluster is limited.[10] Recently, three MOF structures based on Co(II) ions and H_3BTB ligands were reported.[13] Only one of these contained a 6-connected linear trinuclear cluster as an SBU. However, the net topology of the MOF was of low symmetry and was complicated because the MOF had both a linear trinuclear cluster as a 6-connected SBU and an additional dinuclear cluster, $Co_2(COO)_3$, as another type of a 3-connected SBU in the network structure. In the same report, a Co/BTB MOF structure with a 3,6-connected **sit** net topology[14] with μ^3-oxo-bridged triangular trinuclear cobalt clusters, $Co_3O(COO)_4(COOH)_2$, as a distorted trigonal prismatic 6-connected node was also reported. However, there have been no reports on a Co/BTB MOF structure with linear trinuclear $Co_3(COO)_6$ clusters as a 6-connected node.

In this study, using BTB as a C_3 symmetric 3-connected organic node, and one of the most frequently observed cobalt carboxylate clusters, linear trinuclear $Co_3(COO)_6$, as a 6-connected SUB, we report on the synthesis of two new Co/BTB MOF structures having the same 3,6-connected networks but different net topologies, depending on the local point symmetries of the 6-connected SBUs. We also discuss their structural characteristics and gas sorption behavior.

EXPERIMENTAL SECTION

General Procedures. All the reagents used were purchased from commercial sources and used without further purification. Elemental analysis (EA) (C, H, and N) was performed at the Central Research Facilities of the Ulsan National Institute of Science & Technology (Ulsan, Korea). FT-IR spectra were recorded using KBr pellets employing a Nicolet iS10 FT-IR spectrophotometer (4000−400 cm^{-1}). Thermal gravimetric analysis (TGA) data were recorded using a TA Instruments Q-600 series thermal gravimetric analyzer under flowing nitrogen gas with a heating rate of 5 °C min^{-1} between ambient temperature and 550 °C. Powder X-ray diffraction (PXRD) data were recorded using a Rigaku D/M 2200T automated diffractometer at room temperature, with a step size of $2\theta = 0.02°$. During the variable temperature PXRD (VT-PXRD) measurements, the samples were gradually heated from room temperature to the designated temperature in air with a holding time of at least 30 min at each temperature. Simulated PXRD patterns were calculated using the Material Studio software package[15] employing a structural model from single crystal data.

Preparation of $[Co_3(BTB)_2(DMA)_4]$·4DMA (1). A mass of 11.9 mg (0.050 mmol) of $CoCl_2·6H_2O$ and 10.9 mg (0.025 mmol) of H_3BTB was dissolved in 1.25 mL of anhydrous *N*,*N*′-dimethylacetamide (DMA). The resulting solution was transferred into a Pyrex tube. After the tube was sealed tightly, it was heated to 100 °C for 10 days. Rectangular plate-shaped pink crystals were obtained. The crystals were washed with DMA and then air-dried for 1 day. Yield = 8.6 mg, 39%. EA calc for $[Co_3(BTB)_2(DMA)_4]·4DMA$ ($C_{86}H_{102}N_8O_{20}Co_3$, fw = 1744.60 g/mol), **1**. Calc: C = 59.21; H = 5.89; N = 6.42%. Found: C = 58.98; H = 5.79; N = 6.63%. IR (KBr, cm^{-1}): 3427 (m, b), 3271 (vw), 3075 (w), 3034 (w), 2931 (m), 2874 (w, sh), 2815 (vw, sh), 1697 (w, sh), 1641 (vs), 1607 (vs), 1556 (s), 1540 (s), 1509 (m), 1399 (vs), 1305 (m), 1263 (m), 1179 (m), 1141 (w), 1102 (w), 1057 (w), 1016 (m), 965 (vw), 897 (vw), 865 (w), 811 (m), 780 (s), 745 (w), 714 (m), 705 (m), 668 (m), 610 (m), 590 (m), 476 (m), 434 (vw), 419 (vw). The activated sample, **1a**, was prepared by soaking the as-synthesized sample, **1**, in DMA for 1 day, while refreshing the solvent twice during the soaking period, and then vacuum drying at 150 °C for 2−3 days.

Preparation of $[Co_3(BTB)_2(DMA)_2]$·7DMA·3H_2O (2). A mass of 47.6 mg (0.200 mmol) of $CoCl_2·6H_2O$ and 44.6 mg (0.100 mmol) of H_3BTB was dissolved in 5 mL of anhydrous DMA. The resulting solution was transferred into a Pyrex tube. After the tube was tightly sealed, it was heated to 120 °C for 7 days. Block-shaped deep purple crystals were collected, washed with DMA, and then air-dried for 1 day. Yield = 30.9 mg, 32.8%. EA calc for $[Co_3(BTB)_2(DMA)_2]·7DMA·3H_2O$ ($C_{90}H_{117}N_9O_{24}Co_3$, fw = 1885.76 g/mol). **2**. Calc: C = 57.32; H = 6.25; N = 6.68%. Found: C = 57.47; H = 5.97; N = 6.58%. IR (KBr, cm^{-1}): 3405 (s, b), 3269 (m, sh), 3065 (m, sh), 2934 (m), 2876 (w, sh), 2815 (vw, sh), 1695 (w, sh), 1634 (s, sh), 1608 (vs), 1587 (s, sh), 1541 (m), 1512 (m, sh), 1398 (vs), 1306 (w, sh), 1263 (m), 1183 (m), 1143 (vw), 1106 (vw), 1058 (vw), 1016 (m), 964 (vw), 892 (vw), 856 (m), 807 (w), 781 (s), 746 (vw), 705 (m), 669 (m), 595 (w), 479 (m), 419 (vw).

Crystallographic Data Collection and Refinement of the Structures. Crystals of **1** and **2** were coated with Paratone, and the diffraction data were measured at 173 K using Mo Kα radiation in an X-ray diffraction camera system using an imaging plate equipped with a graphite crystal incident beam monochromator. The Rapid Auto software package[16] was used for data collection and processing. Both structures were solved using direct methods employing the XS program of the SHELXTL PLUS software package.[17] The structures were refined using full-matrix least-squares calculations employing the XL program of the SHELXTL PLUS software package.

$[Co_3(BTB)_2(DMA)_4]$·4DMA (1). One ligand, two cobalt sites, with one on a crystallographic inversion center, two ligated DMA, and two lattice DMA solvent molecules formed an asymmetric unit. One ligated DMA molecule and two lattice DMA molecules were statistically disordered. All non-hydrogen atoms were refined anisotropically. The hydrogen atoms were assigned isotropic displacement coefficients U (H) = 1.2U (C) and 1.5U (C_{methyl}), and their coordinates were allowed to ride on their respective atoms. The least-squares refinement of the structural model was performed under geometry restraints and displacement parameter restraints, such as EXYZ, EADP, and ISOR for the disordered DMA molecules. Refinement of the structure converged at final values of $R1$ = 0.0433 and $wR2$ = 0.0829 for 6,342 reflections with $I > 2\sigma(I)$, and $R1$ = 0.0912 and $wR2$ = 0.1099 for all 9,878 reflections. The largest difference for a peak and a hole was 0.600 and −0.765 e·$Å^{-3}$, respectively.

$[Co_3(BTB)_2(DMA)_2]$ (2). One ligand, two cobalt sites, with one on a crystallographic 2-fold rotation axis, a statistically disordered DMA molecule ligated to the cobalt atom with a full occupancy, and a lattice water molecule with a half occupancy formed an asymmetric unit. All non-hydrogen atoms were refined anisotropically. The hydrogen atoms were assigned isotropic displacement coefficients U (H) = 1.2U (C) and 1.5U (C_{methyl}), and their coordinates were allowed to ride on their respective atoms. The hydrogen atoms attached to the water molecules were not included in the least-squares refinement. The least-squares refinement of the structural model was performed under a geometry restraint of DFIX, DANG, and FLAT for the disordered DMA molecule. The final refinement was performed with the modification of the structural factors for the electron densities of the disordered solvent region, including the partially occupied lattice water molecule (3552 $Å^3$, 48.1% of the crystal volume) using the SQUEEZE option of the PLATON software package.[18] Refinement of the structure converged at final values of $R1$ = 0.0800 and $wR2$ = 0.2238 for 3,015 reflections with $I > 2\sigma(I)$, and $R1$ = 0.0872 and $wR2$ = 0.2319 for all 8,672 reflections. The largest differences in the peaks and holes were 0.660 and −0.451 e·$Å^{-3}$, respectively. The Flack parameter value of 0.48(2) obtained indicated that the structure is racemic twined.

A summary of the crystal data for **1** and **2** is given in Table S1 of the Supporting Information.

Gas Sorption Measurements. All the gas sorption isotherms were measured using a BELSORP-max (BEL Japan, Inc.) absorption system employing a standard volumetric technique up to saturated pressure. The N_2 (purity = 99.999%) sorption isotherms were monitored at 77 K. The adsorption data in the pressure range <0.1 P/P_0 were fitted to the Brunauer−Emmett−Teller (BET) equation to determine the BET surface area. The entire set of adsorption data was used to obtain the Langmuir specific surface area. The H_2 (purity =

dx.doi.org/10.1021/cg300686n | Cryst. Growth Des. 2012, 12, 4186−4193

99.9999%) sorption isotherms were measured at 77 K, and the CO_2 (purity = 99.999%) and CH_4 (purity = 99.95%) sorption isotherms were measured at 195 K.

RESULTS AND DISCUSSION

Synthesis of the MOFs. Two different MOFs, $[Co_3(BTB)_2(DMA)_4]$ (**1**) and $[Co_3(BTB)_2(DMA)_2]$ (**2**), were obtained via the solvothermal reaction of $CoCl_2 \cdot 6H_2O$ with H_3BTB (Co(II): H_3BTB = 2:1 molar ratio) in anhydrous DMA under the same reaction conditions described, except for the reaction temperature and the concentration of the reactants used. While **1** was obtained as a pure crystalline product via solvothermal reaction at 100 °C for 10 days, **2** was obtained via the same solvothermal reaction, but at a higher reaction temperature, 120 °C, and a 4-fold higher reactant concentration for 7 days. The reaction used the same reactant concentrations employed for the synthesis of **1**, but it used a higher reaction temperature, 120 °C, which led to the formation of a mixture of crystalline **1** and **2**.

Structural Description of the MOFs. *$[Co_3(BTB)_2(DMA)_4]\cdot 4DMA$ (**1**).* Single crystal structural analysis of **1** revealed that a linear trinuclear cobalt cluster at the crystallographic inversion center with four carboxylate groups in a syn−syn bridging bidentate mode and two carboxylate groups in a μ-carboxylato bridging chelating bidentate mode are interconnected via a 3-connected ligand, BTB (Figure 1). In the trinuclear cluster, the central cobalt(II) ion at the crystallographic inversion center has an octahedral coordination geometry, with six oxygen atoms connected to the six bridging carboxylate groups. The two terminal cobalt(II) ions also have an octahedral coordination geometry, but this is slightly distorted by having four oxygen atoms from three bridging carboxylate groups and two oxygen atoms from the two ligated DMA molecules (Figure 1a and Supporting Information Table S2). The trinuclear cluster serves as a 6-connected node of a compressed trigonal antiprismatic (pseudohexaplanar) geometry (Figure 1b and c). The ligand is a trigonal 3-connected node (Figure 1d), which leads to a corrugated two-dimensional (2-D) layered framework with a 3,6-connected **kgd** net topology (Figure 1e−1h), which is a dual net of the well-known 4-connected Kagomé (**kgm**) net topology.[10] These 2-D layers are stacked in an eclipsed fashion along the crystallographic *a*-axis (Figure 2a and b), and the stacking generates two different types of one-dimensional (1-D) solvent channels along the crystallographic (1, 0, −1) and (1, 0, 1) directions, respectively (Figure 2c and d). The skewed intersection of the two sets of 1-D parallel channels generates three-dimensional (3-D) solvent channels packed with lattice DMA molecules, which comprise approximately 31% (4,328 Å^3) of the total unit cell volume.

Optical microscope photographs of an as-synthesized sample of **1** and the similarity between the powder X-ray diffraction (PXRD) patterns of the as-synthesized crystalline sample and that simulated from the single crystal structural model confirm that the bulk sample was crystalline and pure (Figure S1 of the Supporting Information and Figure 3).

Thermogravimetric analysis of **1** under flowing N_2 gas led to a multistep weight loss (Figure 4). The first 20.2% weight loss up to 150 °C corresponds to the weight loss of four lattice DMA molecules (calculated weight loss of 20.0%) in the solvent channels, and the next two-step 20.3% weight loss up to 340 °C corresponds to the weight loss of four DMA molecules ligated to the two terminal cobalt centers of the 6-connected linear trinuclear cobalt cluster.

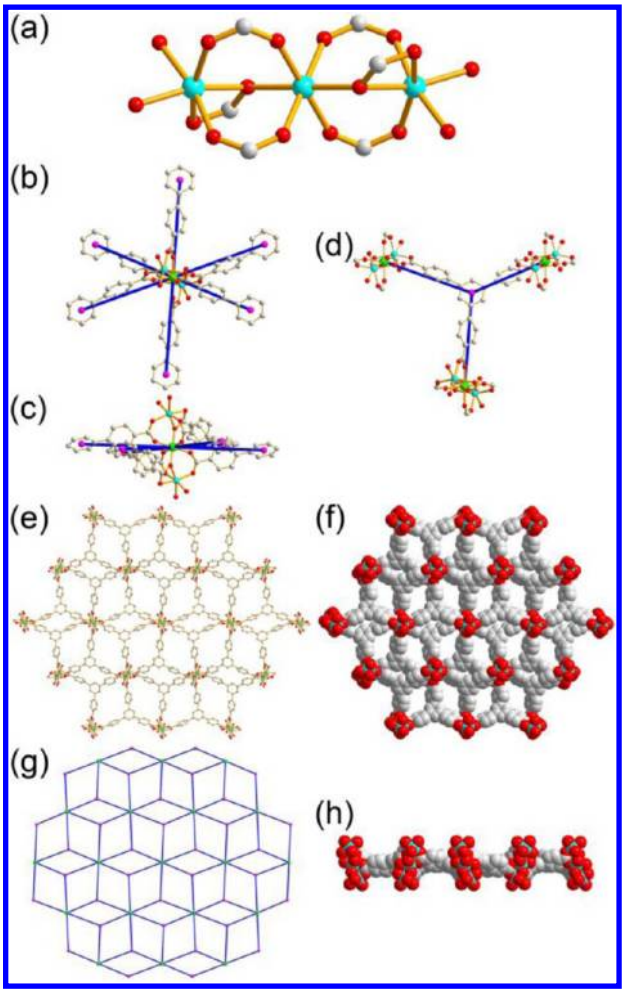

Figure 1. Crystal structure of **1**. (a) Linear trinuclear cobalt cluster as an SBU. A ball-and-stick diagram of the linear trinuclear cobalt cluster as a pseudoplanar 6-connected node with a schematic connectivity to the centers of the six neighboring ligands in (b) top view and (c) side view. (d) Ball-and-stick diagram of the ligand as a 3-connected node with a schematic connectivity with three trinuclear cobalt cluster centers. The 2-D layer viewed along the crystallographic (1, 0, −1) direction using (e) a ball-and-stick model and (f) a space-filling model. (g) Schematic drawing of the 2-D layer showing the 3,6-connected kdg net topology. (h) 2-D layer viewed along the crystallographic (1, 0, 1) direction using a space-filling model.

The VT-PXRD patterns of **1** indicate that the framework structure of the as-synthesized sample is thermally unstable (Figure 5). As the temperature of the sample increases, the PXRD pattern changed and became broadened up to 350 °C, finally losing its crystallinity at 400 °C.

*$[Co_3(BTB)_2(DMA)_2]$ (**2**).* The single crystal structural analysis of **2** also revealed a linear trinuclear cobalt cluster with four carboxylate groups in a syn−syn bridging bidentate mode and two carboxylate groups in a μ-carboxylato bridging chelating bidentate mode interconnected via the 3-connected ligand BTB^{3-} (Figure 6). While the trinuclear cobalt cluster in **1** is at a crystallographic inversion center, the trinuclear cobalt cluster in **2** is on a crystallographic 2-fold rotation axis. The terminal cobalt ions of the trinuclear cobalt cluster in **2** have a 5-coordinate distorted trigonal bipyramidal geometry (Figure 6a and Supporting Information Table S2). The change in symmetry from an inversion point symmetry to a C_2 point symmetry and the distortion of the coordination geometry of

dx.doi.org/10.1021/cg300686n | *Cryst. Growth Des.* 2012, 12, 4186−4193

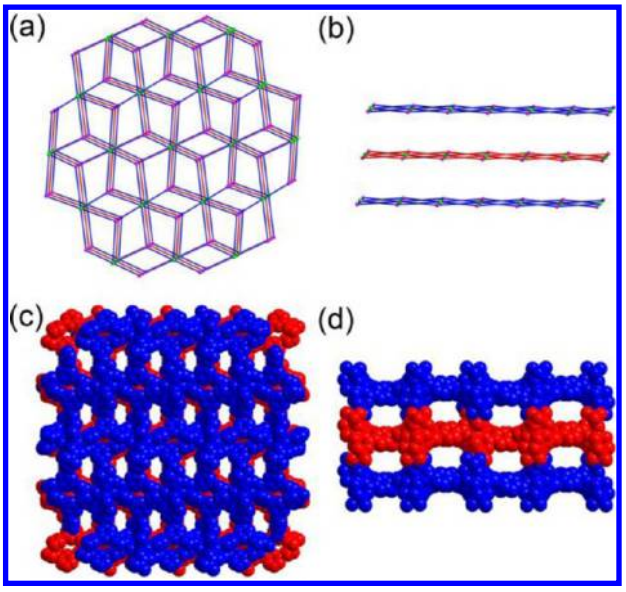

Figure 2. Schematic drawings of the three 2-D layers of **1** viewed along (a) the approximate crystallographic (1, 0, −1) direction and (b) the crystallographic (1, 0, 1) direction. Space-filling diagrams of three 2-D layers of **1** that show two different types of 1-D solvent channels occur along the crystallographic (c) (1, 0, −1) and (d) (1, 0, 1) directions.

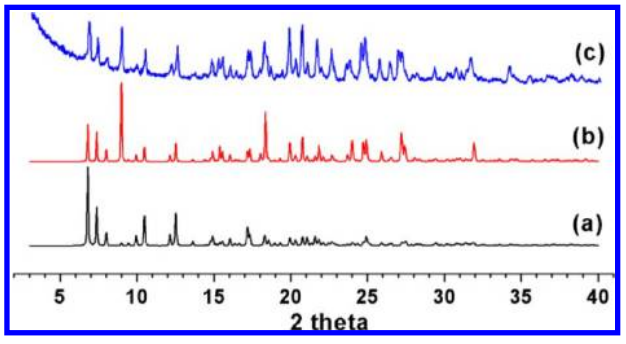

Figure 3. PXRD pattern of **1**. Simulated PXRD patterns of the single crystal structure of **1** with (a) random orientation and (b) (1, 0, −1) preferred orientation of the microcrystalline powder sample. (c) The PXRD pattern of an as-synthesized crystalline sample of **1**.

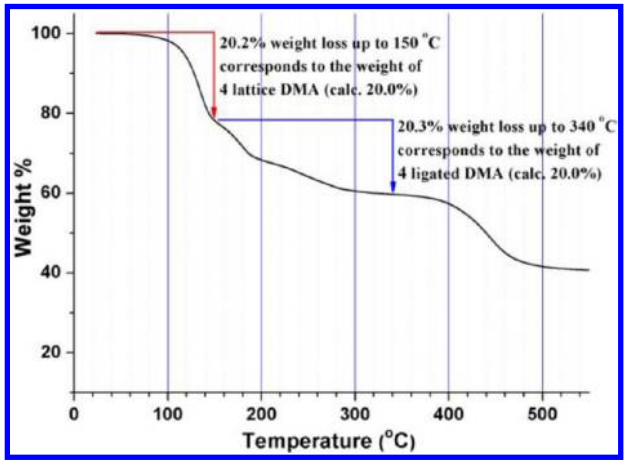

Figure 4. TGA data of **1**.

the terminal cobalt centers from a distorted octahedron to a trigonal bipyramidal geometry lead to the trinuclear cluster of **2** being in a compressed trigonal prismatic (pseudotriangular) 6-

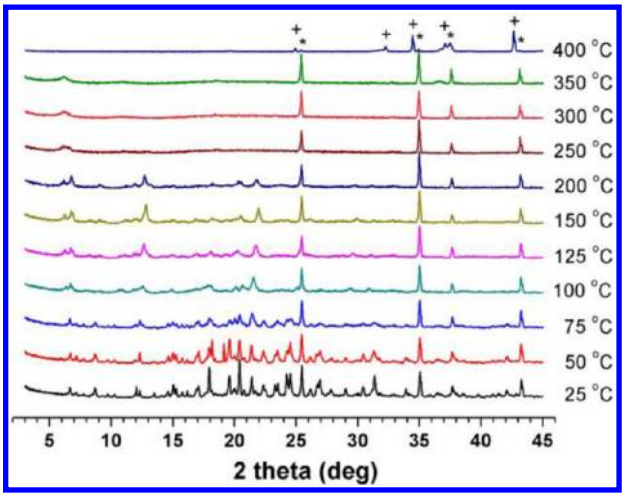

Figure 5. VT-PXRD patterns of **1** in air. The two sets of peaks related to the α-Al_2O_3 high temperature sample holder are denoted by an asterisk and a cross.

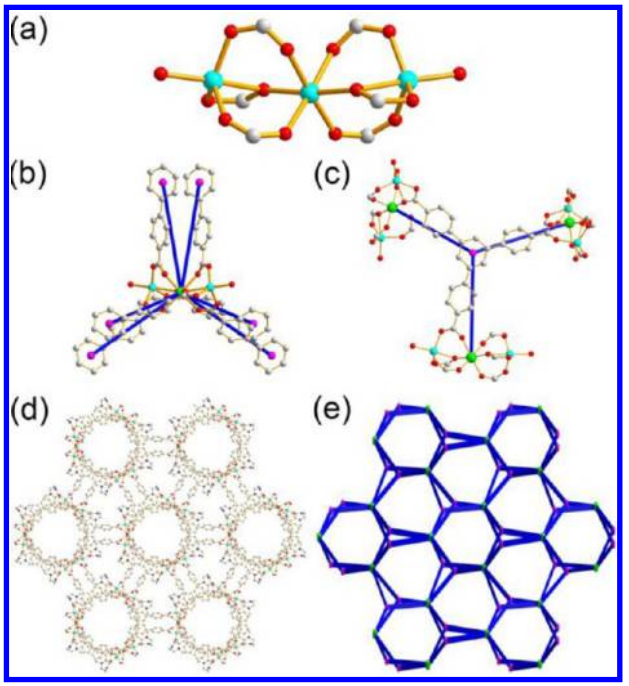

Figure 6. The crystal structure of **2**. (a) The linear trinuclear cobalt cluster as an SBU. (b) A ball-and-stick diagram of the linear trinuclear cobalt cluster as a trigonal prismatic 6-connected node with a schematic connectivity to six ligand centers. (c) A ball-and-stick diagram of the ligand as a planar 3-connected node with a schematic connectivity to three trinuclear cobalt cluster centers. (d) The 3-D framework viewed along the crystallographic (1, 0, −1) direction using a ball-and-stick model. (e) A schematic drawing of the 3-D network showing the unprecedented 3,6-connected net topology with the point symbol $(4^3)_2(4^3{\cdot}12^{12})$.

connected node, while keeping the ligand in the same trigonal 3-connected node (Figure 6b and c).

The combination of a compressed trigonal prismatic 6-connected metal cluster and a trigonal 3-connected ligand resulted in a 3-D network with an unprecedented 3,6-connected net topology and point symbol $(4^3)_2(4^3{\cdot}12^{12})$ (Figure 6d and e).[14] In the binodal 3,6-connected network, the 6-connected trinuclear cobalt clusters are doubly connected

dx.doi.org/10.1021/cg300686n | *Cryst. Growth Des.* 2012, 12, 4186−4193

via the two 3-connected organic ligands, BTB (Figure 7a). The stacking interaction between the ligands contributes to the

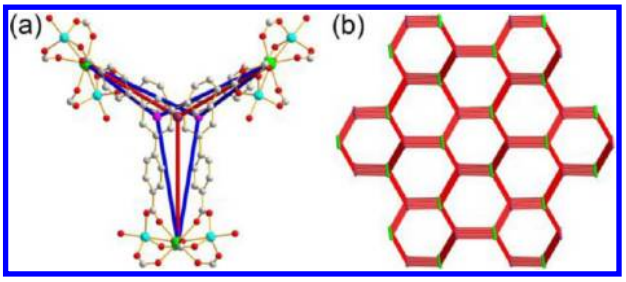

Figure 7. (a) Three trinuclear cobalt clusters doubly interconnected via two 3-connected ligands. (b) Schematic drawing of the uninodal 3-connected network with a twt net topology from two 3-connected nodes simplified to a single 3-connected node.

stabilization of the doubly connected ligand linkage in the network structure (Supporting Information Figure S2 and Table S3). When these doubly connected two 3-connected nodes are simplified as a single 3-connected node, then the network can be considered as a uninodal 3-connected network with a **twt** net topology and point symbol 12^3 (Figure 7b).[14] As expected from the space group of **2**, a $P3_221$, 3_2 helical nature of the network was observed. The trinuclear cobalt clusters are doubly interlinked via the two ligands to form a right-handed *P*-helix with a pitch distance of 26.286 Å along the crystallographic *c*-axis, as shown in Figures 8a and 8b. In the network

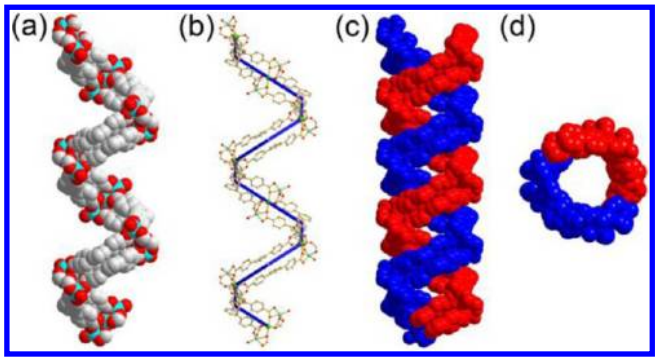

Figure 8. Right-handed *P*-helix along the crystallographic *c*-axis in **2**. (a) A space-filling diagram of a single-stranded helix, (b) a ball-and-stick diagram with a hypothetical helical line, (c) a side view of a double-stranded *P*-helix in a space-filling model with two single-stranded helices in red and blue, and (d) a top view of the double-stranded *P*-helix with the inner channel surrounded by the two single-stranded helices.

structure, two *P*-helices are intertwined to form a double-stranded helix with a half pitch distance of 13.143 Å, acting as a repeat distance along the crystallographic *c*-axis (Figure 8c). The 3-D network of **2** generates two different types of 1-D solvent channel: an inner channel with a double-stranded helix (Type A) and another channel surrounded by the three double-stranded helices (Type B) (Figure 8d and Supporting Information Figure S3). The volume of the solvent channels (3552 $Å^3$) comprises ~48% of the total unit cell volume.

Optical microscopic photographs and powder X-ray diffraction patterns of as-synthesized samples of **2** confirmed that the bulk sample was crystalline and pure and had the same single crystal structure as that of **2** (Figure S1b of the Supporting Information and Figure 9). TGA data of **2** under

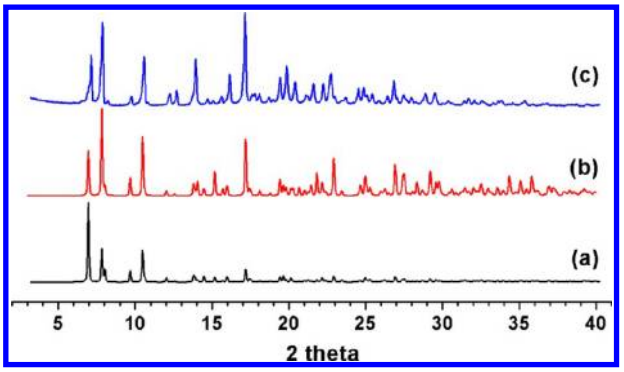

Figure 9. PXRD pattern of **2**. Simulated PXRD patterns using the single crystal structure of **2** with (a) random orientation and (b) (0, 1, 2) preferred orientation of the microcrystalline powder sample are shown. (c) PXRD pattern of the as-synthesized crystalline sample of **2**.

flowing N_2 gas led to a multistep weight loss (Figure 10). The first 35.0% of the weight loss up to 270 °C corresponds to the

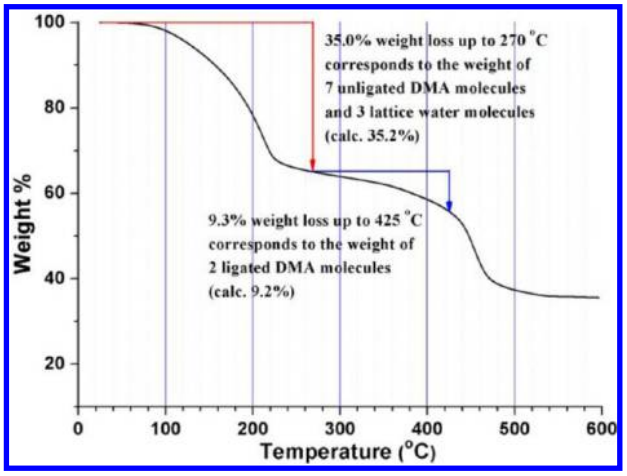

Figure 10. TGA data of **2**.

weight loss of seven unligated DMA molecules and three lattice water molecules (calculated weight loss of 35.2%) contained in the solvent channels. The next weight loss step of 9.3% up to 425 °C corresponds to the weight loss of two ligated DMA molecules (calculated weight loss of 9.2%) before decomposition of the network structure occurs.

The VT-PXRD patterns of **2** indicate that the framework structure of the as-synthesized sample is thermally unstable (Figure 11). As the temperature of the sample increases, the PXRD pattern changes and broadens up to 125 °C, and then finally the sample loses its crystallinity at 250 °C.

Gas Sorption Behavior. The activated sample of **1a** was prepared by keeping as-synthesized **1** in DMA for 1 day while refreshing the solvent twice during soaking and then vacuum drying at 150 °C for 2−3 days. The N_2 sorption isotherms of **1a** at 77 K are shown in Figure 12. The Type I sorption isotherms observed indicate that **1a** has micropores. The BET and Langmuir surface areas calculated from the adsorption isotherms were 320 and 480 $m^2\ g^{-1}$, respectively. The N_2 sorption isotherms showed hysteresis. After an N_2 adsorption of ~70 $cm^3\ g^{-1}$ at ~0.03 P/P_0, the volume of N_2 adsorbed slowly increased up to ~114 $cm^3\ g^{-1}$ at ~0.96P/P_0. Noticeably, the volume of N_2 in the desorption isotherm increased slowly as the pressure decreased, and it reached ~119 $cm^3\ g^{-1}$ at

dx.doi.org/10.1021/cg300686n | *Cryst. Growth Des.* 2012, 12, 4186−4193

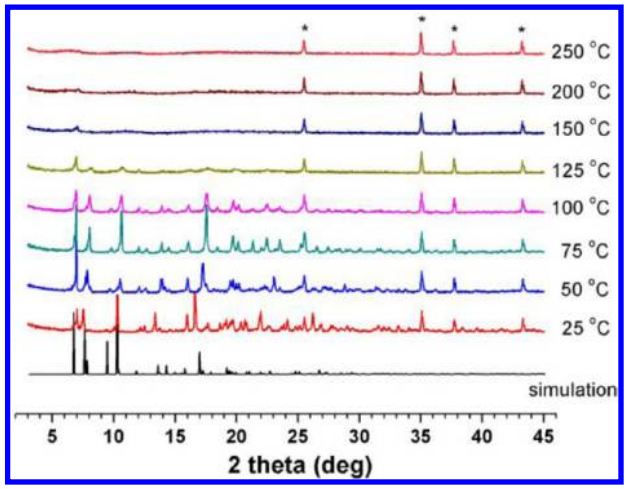

Figure 11. VT-PXRD patterns of **2** in air. The set of peaks related to the α-Al_2O_3 high temperature sample holder is denoted by an asterisk.

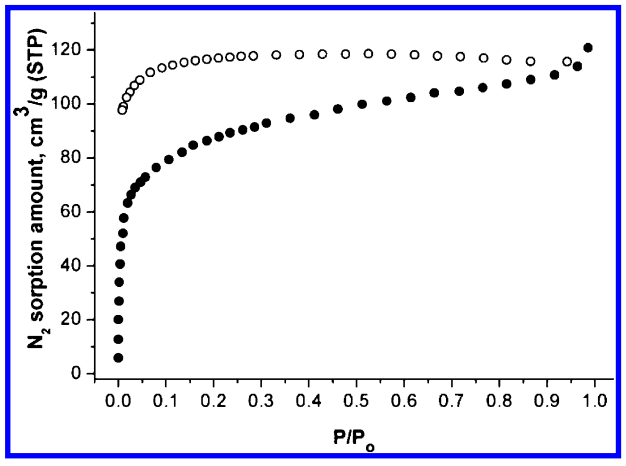

Figure 12. N_2 sorption isotherms of the activated sample, **1a**, at 77 K.

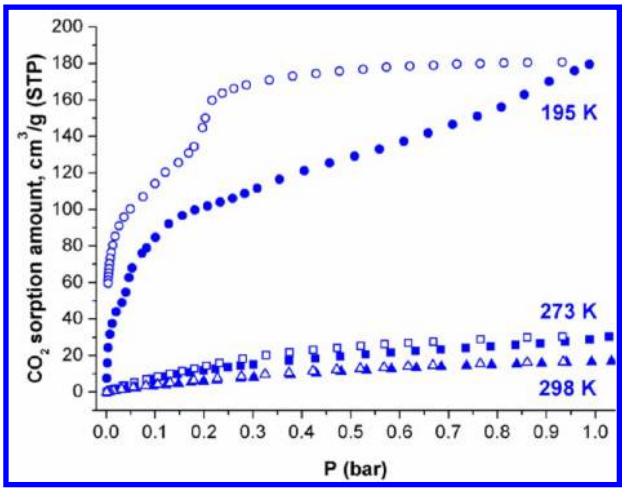

Figure 13. Gas sorption isotherms on the activated sample, **1a**, for CO_2 at 195, 273, and 298 K.

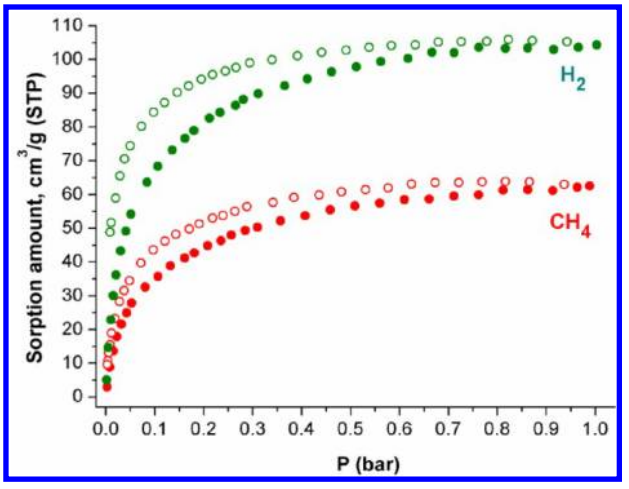

Figure 14. Gas sorption isotherms on the activated sample, **1a**, for H_2 at 77 K and CH_4 at 195 K.

~0.53P/P_0, which is slightly higher than the volume of N_2 adsorbed at ~0.96P/P_0. The flexibility of the framework structure based on the stacked 2-D layers with no appreciable interlayer interactions except for van der Waals interactions and the extremely slow N_2 sorption kinetics are responsible for the hysteresis.[19]

The observed hysteresis of the CO_2 sorption isotherms of **1a** at 195 K also supports the flexibility of the layered framework structure of **1a** (Figure 13). The volume of CO_2 adsorbed on **1a** at 195 K and 1 bar was 180 $cm^3\ g^{-1}$. However, the sorption isotherms at 273 and 298 K showed significantly reduced uptake amounts without any significant hysteresis during adsorption and desorption. The volume of CH_4 and H_2 uptake on **1a** was 63 $cm^3\ g^{-1}$ at 195 K and 104 $cm^3\ g^{-1}$ (0.94 wt %) at 77 K, respectively (Figure 14). The CH_4 sorption isotherms at 195 K and the H_2 sorption isotherms at 77 K also did not show significant hysteresis during adsorption and desorption. When the adsorbate strongly interacted with the framework surface, such as N_2 at 77 K and CO_2 at 195 K, this led to a slight expansion of the accessible pore volume, while adsorbates that weakly interacted with the framework surface, such as CO_2 at 273 and 298 K, CH_4 at 195 K, and H_2 at 77 K, did not cause significant accessible expansion in pore volume.

Several different activation procedures for **2**, including the activation procedure employed for **1a** and a supercritical CO_2 drying procedure, did not show any N_2 and H_2 sorption behavior. The collapse of the pore structure during the activation processes for **2** may be because of the lability of the linear trinuclear cobalt cluster with two 5-coordinate terminal Co(II) ions and ligated DMA molecules.

■ CONCLUSIONS

The reactions of H_3BTB with cobalt chloride hexahydrate in anhydrous DMA solvent at different reactant concentrations and at 100 and 120 °C led to two 3,6-connected MOF structures with two slightly different linear trinuclear $Co_3(COO)_6$ clusters as 6-connected SBUs and the ligand as a 3-connected node. The combination of a 3-connected organic node and a compressed trigonal antiprismatic 6-connected metal cluster with an inversion point symmetry at 100 °C led to the 2-D layered network of **1** with a 3,6-connected **kgd** net topology. On the other hand, a combination of the same 3-connected organic node and a compressed trigonal prismatic 6-connected metal cluster with a 2-fold point symmetry at 120 °C and a 4-fold higher reactant concentration compared with the reactant concentration used for the synthesis of **1** led to an unprecedented 3,6-connected 3-D network of **2** with the point symbol $(4^3)_2(4^3{\cdot}12^{12})$. The 6-connected nodes in the 3,6-

dx.doi.org/10.1021/cg300686n | Cryst. Growth Des. 2012, 12, 4186–4193

connected 3-D network structure are doubly linked via two 3-connected ligands. When the two doubly linked 3-connected nodes are simplified to a topological single 3-connected node, then **2** forms a 3-D network with a uninodal 3-connected **twt** net topology. Slightly different reaction temperatures and reactant concentrations generate two different coordination environments for the terminal cobalt ions of the linear trinuclear cobalt clusters. This difference leads to different local point symmetries of the linear trinuclear cobalt clusters of the compressed trigonal antiprismatic 6-connected node and of the compressed trigonal prismatic 6-connected node, and subsequently, the two different networks have different net topologies.

The flexible network based on the 2-D layered structure of **1a**, with linear trinuclear cobalt clusters for all 6-coordinate metal centers, shows different sorption behavior that is dependent on the adsorbate used and sorption temperature. The adsorbates that are relatively strongly interacting with the framework, such as N_2 at 77 K and CO_2 at 195 K, show a significant hysteresis during adsorption and desorption. On the other hand, the adsorbates that are weakly interacting with the framework, such as CO_2 at 273 and 298 K, H_2 at 77 K, and CH_4 at 195 K, do not show any significant hysteresis during the sorption process. No successful activation procedures were found for the network based on the 3-D layered structure of **2**, with linear trinuclear cobalt clusters having 5−6−5-coordinate metal centers.

Our results suggest that the design and prediction of metal clusters as a rigid SBU for a specific connectivity and local point symmetry are the most important factors in the design and prediction of an MOF with a specific net topology and structure.

■ ASSOCIATED CONTENT

Ⓢ Supporting Information

Cif files for **1** and **2**; a table of the crystal data and structure refinements for **1** and **2**; a table of the selected bond lengths and angles for **1** and **2**; a table of the close contacts between the doubly interconnected two 3-connected ligands of **2** involved in the stacking interaction; optical microscope photographs of **1** and **2** crystals; and a figure showing the stacking interactions between the doubly interconnected two 3-connected ligands of **2**. This material is available free of charge via the Internet at http://pubs.acs.org.

■ AUTHOR INFORMATION

Corresponding Author

*E-mail: mslah@unist.ac.kr.

Notes

The authors declare no competing financial interest.

■ ACKNOWLEDGMENTS

This work was supported by NRF-2011-0027950, NRF-2012-003077, and WCU programs (R31-2011-000-20012-0) through the National Research Foundation of Korea.

■ ABBREVIATIONS

MOF = metal−organic framework; SBU = secondary building unit; EA = elemental analysis; TGA = thermal gravimetric analysis; PXRD = powder X-ray diffraction; VT-PXRD = variable temperature PXRD; BET = Brunauer−Emmett−Teller; H_3BTB = 1,3,5-benzenetribenzoic acid; DMA = *N*,*N*′-dimethylacetamide

■ REFERENCES

(1) O'Keeffe, M.; Yaghi, O. M. *Chem. Soc. Rev.* **2012**, *112*, 675−702.

(2) (a) Li, H.; Eddaoudi, M.; O'Keeffe, M.; Yaghi, O. M. *Nature* **1999**, *402*, 276−279. (b) Eddaoudi, M.; Kim, J.; Rosi, N.; Vodak, D.; Wachter, J.; O'Keeffe, M.; Yaghi, O. M. *Science* **2002**, *295*, 469−472. (c) Yaghi, O. M.; O'Keeffe, M.; Ockwig, N. W.; Chae, H. K.; Eddaoudi, M.; Kim, J. *Nature* **2003**, *423*, 705−714. (d) Rosi, N. L.; Eckert, J.; Eddaoudi, M.; Vodak, D. T.; Kim, J.; O'Keeffe, M.; Yaghi, O. M. *Science* **2003**, *300*, 1127−1129.

(3) (a) Chui, S. S.-Y.; Lo, S. M.-F.; Charmant, J. P. H.; Orpen, A. G.; Williams, I. D. *Science* **1999**, *283*, 1148−1150. (b) Wang, X.-S.; Ma, S.; Sun, D.; Parkin, S.; Zhou, H.-C. *J. Am. Chem. Soc.* **2006**, *128*, 16474−16475. (c) Ma, S.; Sun, D.; Ambrogio, M.; Fillinger, J. A.; Parkin, S.; Zhou, H.-C. *J. Am. Chem. Soc.* **2007**, *129*, 1858−1859. (d) Wang, X.-S.; Ma, S.; Yuan, D.; Yoon, J. W.; Hwang, Y. K.; Chang, J.-S.; Wang, X.; Jørgensen, M. R.; Chen, Y.-S.; Zhou, H.-C. *Inorg. Chem.* **2009**, *48*, 7519−7521.

(4) O'Keeffe, M.; Peskov, M. A.; Ramsden, S. J.; Yaghi, O. M. *Acc. Chem. Res.* **2008**, *41*, 1782−1789.

(5) (a) Chae, H. K.; Siberio-Pérez, D. Y.; Kim, J.; Go, Y.; Eddaoudi, M.; Matzger, A. J.; O'Keeffe, M.; Yaghi, O. M. *Nature* **2004**, *427*, 523−527. (b) Kim, J.; Chen, B.; Reineke, T. M.; Li, H.; Eddaoudi, M.; Moler, D. B.; O'Keeffe, M.; Yaghi, O. M. *J. Am. Chem. Soc.* **2001**, *123*, 8239−8247. (c) Caskey, S. R.; Wong-Foy, A. G.; Matzger, A. J. *Inorg. Chem.* **2008**, *47*, 7751−7756. (d) Hou, L.; Zhang, J.-P.; Chen, X.-M.; Ng, S. W. *Chem. Commun.* **2008**, 4019−4021.

(6) (a) Chen, B.; Eddaoudi, M.; Hyde, S. T.; O'Keeffe, M.; Yaghi, O. M. *Science* **2001**, *291*, 1021−1023. (b) Mu, B.; Li, F.; Walton, K. S. *Chem. Commun.* **2009**, 2493−2495.

(7) (a) Choi, S. B.; Seo, M. J.; Cho, M.; Kim, Y.; Jin, M. K.; Jung, D.-Y.; Choi, J.-S.; Ahn, W.-S.; Rowsell, J. L. C.; Kim, J. *Cryst. Growth Des.* **2007**, *7*, 2290−2293. (b) Devic, T.; Serre, C.; Audebrand, N.; Marrot, J.; Férey, G. *J. Am. Chem. Soc.* **2005**, *127*, 12788−12789. (c) Volkringer, C.; Loiseau, T.; Marrot, J.; Férey, G. *CrystEngComm* **2009**, *11*, 58−60. (d) Sumida, K.; Hill, M. R.; Horike, S.; Dailly, A.; Long, J. R. *J. Am. Chem. Soc.* **2009**, *131*, 15120−15121.

(8) Tranchemontagne, D. J.; Mendoza-Cortés, J. L.; O'Keeffe, M.; Yaghi, O. M. *Chem. Soc. Rev.* **2009**, *38*, 1257−1283.

(9) (a) Choi, E.-Y.; Park, K.; Yang, C.-M.; Kim, H.; Son, J.-H.; Lee, S. W.; Lee, Y. H.; Min, D.; Kwon, Y.-U. *Chem.—Eur. J.* **2004**, *10*, 5535−5540. (b) Chun, H.; Jung, H.; Seo, J. *Inorg. Chem.* **2009**, *48*, 2043−2047. (c) Chen, P.-K.; Qi, Y.; Che, Y.-X.; Zheng, J.-M. *CrystEngComm* **2010**, *12*, 720−724. (d) Gong, Y.; Hu, C. W.; Li, H.; Huang, K. L.; Tang, W. *J. Solid State Chem.* **2005**, *178*, 3152−3158. (e) Hilderbrand, S. A.; Lippard, S. J. *Inorg. Chem.* **2004**, *43*, 5294−5301.

(10) (a) Gavrilenko, K. S.; Punin, S. V.; Cador, O.; Golhen, S.; Ouahab, L.; Pavlishchuk, V. V. *J. Am. Chem. Soc.* **2005**, *127*, 12246−12253. (b) Bu, X.-H.; Tong, M.-L.; Xie, Y.-B.; Li, J.-R.; Chang, H.-C.; Kitagawa, S.; Ribas, J. *Inorg. Chem.* **2005**, *44*, 9837−9846. (c) Gavrilenko, K. S.; Gal, Y. L.; Cador, O.; Golhen, S.; Ouahab, L. *Chem. Commun.* **2007**, 280−282. (d) Sun, D.; Ma, S.; Ke, Y.; Petersen, T. M.; Zhou, H.-C. *Chem. Commun.* **2005**, 2663−2665. (e) Chen, Z.-F.; Zhang, Z.-L.; Tan, Y.-H.; Tang, Y.-Z.; Fun, H.-K.; Zhou, Z.-Y.; Abrahams, B. F.; Liang, H. *CrystEngComm* **2008**, *10*, 217−231. (f) Wang, X.; Liu, L.; Conato, M.; Jacobson, A. J. *Cryst. Growth Des.* **2011**, *11*, 2257−2263. (g) Zhou, H.; Chu, C.-X.; Li, Y.-Z. *Acta Crystallogr.* **2011**, *E67*, m841−m842. (h) Kim, E. Y.; Song, Y. J.; Koo, H. G.; Lee, J. H.; Park, H. M.; Kim, C.; Kwon, T.-H.; Huh, S.; Kim, S.-J.; Kim, Y. *Polyhedron* **2010**, *29*, 3335−3341. (i) Hu, D.-X.; Chen, P.-K.; Luo, F.; Xue, L.; Che, Y.; Zheng, J.-M. *Inorg. Chim. Acta* **2007**, *360*, 4077−4084.

(11) (a) Cheng, D.; Khan, M. A.; Houser, R. P. *Cryst. Growth Des.* **2004**, *4*, 599−604. (b) Ma, L.-F.; Wang, Y.-Y.; Wang, L.-Y.; Lu, D.-H.; Batten, S. R.; Wang, J.-G. *Cryst. Growth Des.* **2009**, *9*, 2036−2038. (c) Lim, C.-S.; Schnobrich, J. K.; Wong-Foy, A. G.; Matzger, A. J. *Inorg. Chem.* **2010**, *49*, 5271−5275. (d) Chen, Q.; Lin, J.-B.; Xue, W.;

Zeng, M.-H.; Chen, X.-M. *Inorg. Chem.* **2011**, *50*, 2321−2328. (e) Kiskin, M. A.; Aleksandrov, G. G.; Bogomyakov, A. S.; Novotortsev, V. M.; Eremenko, I. L. *Inorg. Chem. Commun.* **2008**, *11*, 1015−1018. (f) Sumner, C. E., Jr.; Steinmetz, G. R. *Inorg. Chem.* **1989**, *28*, 4290−4294. (g) Pakhmutova, E. V.; Sidorov, A. A.; Fomina, I. G.; Aleksandrov, G. G.; Novotortsev, V. M.; Ikorskii, V. N.; Eremenko, I. L. *Russ. Chem. Bull., Int. Ed.* **2003**, *52*, 2125−2131. (h) Milios, C. J.; Prescimone, A.; Sanchez-Benitez, J.; Parsons, S.; Murrie, M.; Brechin, E. K. *Inorg. Chem.* **2006**, *45*, 7053−7055. (i) Alborés, P.; Rentschler, E. *Angew. Chem., Int. Ed.* **2009**, *48*, 9366−9370.

(12) (a) Jaitner, P.; Rieker, C.; Wurst, K. *Chem. Commun.* **1997**, 1245−1246. (b) Aromí, G.; Batsanov, A. S.; Christian, P.; Helliwell, M.; Roubeau, O.; Timco, G. A.; Winpenny, R. E. P. *Dalton Trans.* **2003**, 4466−4471. (c) Pakhmutova, E. V.; Sidorov, A. A.; Fomina, I. G.; Aleksandrov, G. G.; Novotortsev, V. M.; Ikorskii, V. N.; Eremenko, I. L. *Russ. Chem. Bull., Int. Ed.* **2003**, *52*, 2125−2131. (d) Dell'Amico, D. B.; Calderazzo, F.; Giovannitti, B.; Pelizzi, G. *J. Chem. Soc., Dalton Trans.* **1984**, 647−652. (e) Lewis, G. E.; Kraihanzel, C. S. *Inorg. Chem.* **1983**, *22*, 2895−2899. (f) Livage, C.; Guillou, N.; Chaigneau, J.; Rabu, P.; Drillon, M.; Férey, G. *Angew. Chem., Int. Ed.* **2005**, *44*, 6488−6491. (g) Ackermann, H.; Leo, R.; Massa, W.; Dehnicke, K. *Z. Naturforsch.* **1998**, *53b*, 1241−1243. (h) Beattie, J. K.; Hambley, T. W.; Klepetko, J. A.; Masters, A. F.; Turner, P. *Polyhedron* **1997**, *16*, 2109−2112. (i) Chiesa, A.; Ugo, R.; Sironi, A.; Yatsimirski, A. *J. Chem. Soc., Chem. Commun.* **1990**, 350−351. (j) Papaefstathiou, G. S.; Perlepes, S. P.; Escuer, A.; Vicente, R.; Font-Bardia, M.; Solans, X. *Angew. Chem., Int. Ed.* **2001**, *40*, 884−886. (k) Tsohos, A.; Dionyssopoulou, S.; Raptopoulou, C. P.; Terzis, A.; Bakalbassis, E. G.; Perlepes, S. P. *Angew. Chem., Int. Ed.* **1999**, *38*, 983−985. (l) Boudalis, A. K.; Donnadieu, B.; Nastopoulos, V.; Clemente-Juan, J. M.; Mari, A.; Sanakis, Y.; Tuchagues, J.-P.; Perlepes, S. P. *Angew. Chem., Int. Ed.* **2004**, *43*, 2266−2270.

(13) Wollmann, P.; Leistner, M.; Stoeck, U.; Grünker, R.; Gedrich, K.; Klein, N.; Throl, O.; Grählert, W.; Senkovska, I.; Dreisbach, F.; Kaskel, S. *Chem. Commun.* **2011**, *47*, 5151−5153.

(14) Blatov, A. *IUCr CompComm Newsletter*; 2006, 7, 4, TOPOS is available at http://www.topos.ssu.samara.ru/.

(15) *Materials Studio program*, version 4.3; Accelrys: San Diego, CA, 2008.

(16) *Rapid Auto software*, R-Axis series; Rigaku Corporation: Cat. No. 9220B101.

(17) Sheldrick, G. M. *SHELXTL-PLUS, Crystal Structure Analysis Package*; Bruker Analytical X-Ray: Madison, WI, USA, 1997.

(18) PLATON program: Spek, A. L. *Acta Crystallogr., Sect. A* **1990**, *46*, 194−201.

(19) Maji, T. K.; Matsuda, R.; Kitagawa, S. *Nat. Mater.* **2007**, *6*, 142−148.